Pharm Res (2012) 29:3347–3361
DOI 10.1007/s11095-012-0830-5

RESEARCH PAPER

Fatty Acid–RGD Peptide Amphiphile Micelles as Potential Paclitaxel Delivery Carriers to $\alpha_v\beta_3$Integrin Overexpressing Tumors

Narashima Murthy Javali • April Raj • Poonam Saraf • Xiaoling Li • Bhaskara Jasti

Received: 28 April 2012 / Accepted: 5 July 2012 / Published online: 24 July 2012

ABSTRACT

Purpose To design and synthesize fatty acid-RGD peptide amphiphiles with ADA linker for their potential delivery of hydrophobic drugs like paclitaxel targeted to $\alpha_v\beta_3$ integrin overexpressing tumors.

Methods Four amphiphiles - C16 or C18 fatty acid–RGD peptide and ADA linker were designed and synthesized. CMC, size and zeta potential of the amphiphiles were determined. FITC loaded micelles uptake into A2058 melanoma cells was investigated at 4°C and 37°C using confocal microscopy. Paclitaxel was loaded into micelles, their encapsulation efficiency and cytotoxicity of micelles was evaluated. The stability of the micelles was determined using FRET method.

Results Mass, ^{1}H NMR and HPLC analysis confirmed the formation of amphiphiles and their purity. Among the amphiphiles, C18-$(ADA)_2$-RGD amphiphile exhibited lowest CMC ($9.00 \pm 1.73\ \mu$M) and its micelles had suitable size (194.63 ± 44.86 nm) and zeta potential (0.27 ± 1.96 mV) for targeting. The cellular uptake of the micelles was temperature dependent and the micelles were stable. The IC50 of paclitaxel loaded in micelles decreased 50% in $\alpha_v\beta_3$ integrin overexpressing cells and showed a 4 fold increase in normal cells when compared to free paclitaxel.

Conclusion Amphiphiles of fatty acids–ADA-RGD were synthesized. These amphiphiles formed stable micelles and were effective as targeted delivery carriers to $\alpha_v\beta_3$ integrin overexpressing tumors.

Electronic supplementary material The online version of this article (doi:10.1007/s11095-012-0830-5) contains supplementary material, which is available to authorized users.

N. M. Javali • A. Raj • P. Saraf • X. Li • B. Jasti (✉)
Department of Pharmaceutics & Medicinal Chemistry,
Thomas. J. Long School of Pharmacy & Health Sciences,
University of the Pacific
Stockton, California, USA
e-mail: bjasti@pacific.edu

A. Raj
Department of Biological Sciences, University of the Pacific
Stockton, California, USA

KEY WORDS cytotoxicity · paclitaxel · peptide amphiphile · RGD · $\alpha_v\beta_3$ integrin

INTRODUCTION

Peptide amphiphiles (PA) are molecular structures composed of either hydrophobic and hydrophilic domains in peptide itself or a peptide that is conjugated to long chain alkyl moieties. PAs are biocompatible, biodegradable and easy to synthesize. Their amphiphilic nature renders them to self-assemble into nanostructures above the critical micellar concentration (CMC) in aqueous media. During the self-assembly, hydrophobic segments assemble to form inner core of the nanostructure and hydrophilic segments are displaced into outer surface to have hydrophilic interaction with aqueous surroundings. This free energy driven aggregation behaviour is enhanced by intermolecular hydrophobic interactions and hydrogen bonding while electrostatic repulsion disfavours it. The self-assembly leads to formation of different kinds of nanostructures like micelles (1), nanofibers (2), ribbons (3), nanotubes (4) and nanobelts (5). Morphology of the nanostructures can be tuned by altering structure of PA, amino acid sequence and assembly atmosphere (1,6–8). β-sheet forming peptide linkers between hydrophobic chain and bioactive peptide, facilitate intermolecular hydrogen bonding and bring on assembly of one-dimensional nanofibers, which arrange themselves into a three-dimensional gel network and these have proved their efficiency in the delivery of bone marrow mononuclear cells (BMNCs) (9), sonic hedgehog (SHH) (10), angiogenic factors such as vascular endothelial growth factor (VEGF), and basic fibroblast growth factor (FGF_2) (11) for tissue engineering and regenerative medicine. PA nanofibers were also utilized for controlled release of antisense oligonucleotides (12) and genetic materials (13).

For the above applications, therapeutic agents are embedded in the self-assembled fibrillar hydrogel structure formed by intermolecular hydrogen bonding of the peptide segment assisted by multivalent ions. Another event that occurs during the course of self-assembly is the collapse of hydrophobic segment spontaneously creating tiny dense hydrophobic pockets in aqueous environment. This presents an ideal scenario to encapsulate hydrophobic molecules inside the core of nanostructures. Such non-covalent entrapment of hydrophobic drugs eliminates the need for covalent conjugation of drugs to carrier. Even though applications of PA nanostructures were extensively studied for delivery of cells and proteins, science of drug delivery with PA nanostructures is still in its infancy. Reasons for limited use of PA nanostructures in drug delivery are cost of production, difficulties related to prediction of size and shape of nanostructures formed after self-assembly and lack of quantitative drug encapsulation efficiency to achieve desired biological effect. The encapsulation and delivery of model hydrophobic molecules like pyrene (14), porphyrin (15) and doxorubicin (13,16) inside the hydrophobic core of the self-assembled PA nanostructures were demonstrated but limited in number. In addition, the ability of self-assembled nanostructures to display bioactive peptide epitopes in outer shell surface provides a unique opportunity for active targeting. Active targeted drug delivery is based on the interaction of ligands on drug delivery vehicle with targeted biomolecules, which are overexpressed in disease state cells than normal cells. One such broadly studied system for active targeting of tumor endothelium is interaction between Arg-Gly-Asp (RGD) peptide epitome and $\alpha_v\beta_3$ integrin. The RGD tripeptide sequence found in the extracellular matrix proteins including vitronectin, fibronectin and collagen, plasma proteins such as fibrinogen is recognised by $\alpha_v\beta_3$ integrin to induce diverse biological processes (17). The $\alpha_v\beta_3$ integrin is heterodimeric glycosylated protein made up of 125 kDa α_v subunit and a 105 kDa β_3 subunit and is implicated in tumour angiogenesis, metastasis and invasion (18,19). It is overexpressed in variety of cancer cells including melanoma, glioblastoma, breast, prostate, cervical, ovarian and pancreatic cancers.

Active targeting to integrin overexpressing cells using liposome prepared from lipopeptides was studied by Hölig *et al.* (20). The lipopeptides consisted of a 1,2 dipalmitoyl-glycero-3-succinyllysine and RGD10 motif demonstrated high binding with short circulation half-life and exhibited rapid elimination from blood stream which was shortcoming of the system. In comparison to the liposome system, PAs micelles are easy to formulate and their *in vivo* stability as well as circulation half-life can be improved by controlling the size and zeta potential of the micelles also by modulating the hydrophilic and lipophilic balance (HLB) of the amphiphiles. PAs of RGD peptide and fatty acids, including capric acid (C10), lauric acid (C12), myristic acid (C14), palmitic acid (C16), stearic acid (C18) were designed and synthesized in our laboratory. The data indicated that C16-RGD and C18-RGD amphiphiles were able to self-assemble into nanostructures and paclitaxel loaded nanostructures were able to bind specifically to $\alpha_v\beta_3$ integrin overexpressing tumor cells (21). However, these amphiphiles were extremely hydrophobic posing challenges in their evaluation as vehicles for drug delivery. Use of hydrophilic linkers in the PA of C16 and C18 fatty acids conjugated with RGD is hypothesized to improve hydrophilicity and enhance micellar formation. Oligo ethylene glycol linkers such as 8-amino-3,6-dioxaoctanoic acid (ADA), are known to improve both hydrophilicity and biological profile of peptide conjugates (16,22). The HLB of the PA can be tuned by varying the number of ADA units. Furthermore, such poly ethylene glycol (PEG) related compounds are approved by the FDA to use in the formulations because PEG is non-toxic, does not produce immunogenic responses and is safely eliminated from the body. Additionally, PEG solubilises in both organic and aqueous solvents with low polydispersity.

Hydrophobic anticancer drug paclitaxel is extensively used anticancer drug and approved for the treatment of solid tumors of ovary, breast, and lung, acute leukaemia and neck carcinoma. Clinical use of paclitaxel suffered from serious adverse effects such as neutropenia and peripheral sensory neuropathy developed during the course of treatment (23). Paclitaxel is available for intravenous administration in a micellar formulation with Cremophor EL. However, this formulation is known to cause severe hypersensitivity reactions (24). To overcome the problems associated with physicochemical properties and to circumvent side effects, RGD decorated polymeric micelles (25,26) and polymeric nanoparticles (27,28) loaded with paclitaxel were studied for active targeted drug delivery. Findings from these experiments revealed that decoration of paclitaxel loaded drug delivery vehicle with RGD peptide significantly enhanced paclitaxel bioavailability, specificity and efficacy than free drug in tumor active targeting. However, conventional amphiphilic copolymers used in these formulations are nonbiodegradable causing long term toxicity, lack of specificity and induce haemolysis in red blood cells (RBC) by colloid osmotic lysis (29). Therefore, there is significant scope for the development of novel drug delivery systems for paclitaxel with improved pharmacokinetics profile, less toxicities as well as better active targeting capability.

In this study, PAs of RGD peptide with C16 and C18 fatty acids, containing one or two units of ADA linker in between RGD peptide and fatty acid were designed, synthesized and characterized for their CMC. The self-assembled micelles were characterized for their size and zeta potential. The cellular uptake of the fluorescein isothiocyanate (FITC) loaded C18-$(ADA)_2$-RGD micelles was studied

using confocal microscopy and evaluated for their ability to enhance solubility of the hydrophobic anticancer drug paclitaxel. The cytotoxicity of paclitaxel loaded micelles in comparison with free paclitaxel was determined in A2058 melanoma cells and Detroit 551 keratinocyte cells with sulforhodamine B (SRB) assay. Kinetic stability of the micelles was studied by förster resonance energy transfer (FRET) analysis.

MATERIALS AND METHODS

Materials

The Wang resin preloaded with Fmoc-Asp (OtBu)-OH and piperidine were purchased from Advanced Chemtech (Louisville, KY, USA). Fmoc-Gly-OH, Fmoc-Arg(Pbf)-OH, triisopropylsilane (TIS), *N*-hydroxybenzotriazole (HOBT), 2-(1H-7-azabenzotriazol-1-yl)-1,1,3,3-tetramethyluronium hexafluorophosphate (HATU), ADA and benzotriazol-1-yl-oxytripyrrolidinophosphonium hexafluorophosphate (PyBOP) were brought from Chem-Impex International Ltd(Wood Dale, IL, USA). Diethyl ether, trifluoroacetic acid (TFA), diisopropylethylamine (DIPEA), *N*,*N*′-diisopropylcarbodiimide (DIC), *N*,*N*′-dimethylformamide (DMF), stearic acid and palmitic acid were all obtained from Acros Organics (New Jersey, USA). Acetonitrile (ACN) and dichloromethane (DCM) were purchased from Fisher Scientific (Pittsburgh, PA, USA). Pyrene and SRB assay kit were obtained from Sigma-Aldrich (St. Louis, MO, USA). Paclitaxel was purchased from LC laboratories (Woburn, MA, USA). The fluorescent probe FITC was obtained from Calbiochem (San Diego, CA, USA). Alexa-Fluor 594 wheat germ agglutinin, SlowFade®, 1,1′-dioctadecyl-3,3,3,3′-tetramethylindocarbocyanine perchlorate (DiI) and 3,3′-dioctadecyloxacarbocyanine perchlorate (DiO) were purchased from Invitrogen (Carlsbad, CA, USA). All chemicals and solvents were used without further purification.

Cell Culture

A2058 melanoma cells and Detroit 551 keratinocyte cells were obtained from ATCC (Manassas, VA, USA). The A2058 melanoma cells were cultured in dulbecco's modified eagle medium (DMEM, Invitrogen corporation, Carlsbad, CA) containing 10% heat inactivated fetal bovine serum, 1% L-Glutamine (200 mM, Gibco, Invitrogen corporation, Japan) and 1% penicillin-streptomycin (5000 I.U./mL, Cellgro, Mediatech Inc, VA). Detroit 551 keratinocyte cells were cultured in eagle's minimum essential medium (EMEM, ATCC, USA) supplemented with 10% fetal bovine serum, 1% L-Glutamine (200 mM, Gibco, Invitrogen corporation, Japan) and 1% penicillin-streptomycin (5000 I.U./mL, Cellgro, Mediatech Inc, VA). Both cell lines were incubated in a humidified environment at 37°C and 5% CO_2. Cells were used for experiments when they reached a confluency of approximately 80–85%.

Synthesis of Peptide Amphiphiles

The amphiphiles were synthesized employing the standard Fmoc/tBu chemistry protocols. The synthesis was carried out on Wang resin preloaded with Fmoc-Asp (OtBu)-OH (0.8 mmol/gm substitution) at 0.4 mmol scale. RGD peptide was built by coupling of Fmoc protected amino acid monomers, Fmoc-gly-OH and Fmoc-Arg(Pbf)-OH using Fmoc-amino acids (3 equiv), DIC (3 equiv) and HOBT (3 equiv) in DMF (8 mL) and shaking for 2 h. Once the RGD peptide synthesis was completed, one or two units of ADA linker were conjugated to amino group of arginine. This conjugation was carried out with ADA (3 equiv), HATU (3 equiv), HOBT (3 equiv) and DIPEA (4 equiv) in DMF (8 mL) and shaking for 3 h. Amino group of ADA unit was acylated with C16 or C18 fatty acid using fatty acid (3 equiv), PyBOP (3 equiv) and DIPEA (4 equiv) in the 50:50 mixture of DMF: DCM (8 mL) and shaking for 3 h. During the entire synthesis Fmoc group deprotection was carried out using solution of 20% piperidine in DMF (2×8 mL) and shaking for 3 min and 30 min, respectively. After each acylation and deprotection reaction, the resin was washed with DMF (3×8 mL) and DCM (3×8 mL) and shaking each time for 2 min. The coupling and deprotection reactions were monitored by performing the Kaiser test (approximately 10 beads treated with 1 drop of each three Kaiser test reagents and heated at 100°C, deprotection of Fmoc group lead to a positive Kaiser test, indicated by the development of a blue colour, while completion of coupling yielded a negative test, demonstrated by the development of a yellow colour). Assembled PA cleavage and deprotection of side chain protection groups were performed by treating with cleavage cocktail, containing TFA, deionized water and TIS in the 95:2.5:2.5 ratios. After shaking for 3 h, the TFA solution was collected and concentrated by rotary evaporation at 30°C. The viscous solution was cooled to −10°C and cold diethyl ether was added to precipitate the PA. Precipitate was collected through filtration, washed with cold diethyl ether and cold deionized water and further dissolved in the 50:50 mixture of ACN and water followed by lyophilization. Dried PAs were stored at −20°C until their further use. The purity of the PA was determined by high pressure liquid chromatography (HPLC) using Waters 2690 Separations Module HPLC system (Waters Corp, Milford, USA) equipped with photodiode array model 996 detector and Phenomenex Gemini C18 column (Phenomenex, Torrance, USA) having 250×4.6 mm dimensions. The mobile phase solvents used were water with 0.1% TFA (A) and ACN with 0.1% TFA (B), elution was performed with linear gradient

from 40 to 60% B over 10 min at 1.0 mL/min flow rate and from 60 to 80% B over next 5 min at 1.0 mL/min flow rate. The same gradient was maintained further for 10 min at 1.0 mL/min flow rate and back to 40% B in last 10 min of analysis to achieve equilibrium for the next injection. The peak area was measured at 210 nm. Mass spectral analysis was carried out on Varian 1200 LC-MS electron spray ionization (ESI) mass spectrometer (Varian Inc, Walnut Creek, USA). ^{1}H NMR was performed with JEOL ECA 600 MHz NMR instrument (JEOL USA Inc, MA, USA).

Determination of Critical Micellar Concentration

Critical micellar concentration was measured with fluorescence spectroscopy using pyrene as fluorescence probe. Briefly, a stock solution of 2 mg/mL of amphiphile was prepared in methanol. Different volumes of this stock along with 50 μL of 1.8×10^{-4} M solution of pyrene in DCM were added to 20 mL vials and vortexed thoroughly. Organic solvents were evaporated and 15 mL of distilled water was added to the amphiphile and pyrene film, yielding a final amphiphile concentrations ranging from approximately 0.2 to 120 μM as well as pyrene concentration of 6.0×10^{-7} M. Samples were then equilibrated for 24 h at 37°C and 85 rpm. Pyrene emission spectrum was recorded with Shimadzu RF-5301 PC spectrofluorometer (Shimadzu Corporation, Pleasanton, USA) using an excitation wavelength of 337 nm and emission spectra ranging from 350 to 500 nm. The first (I_1) and third (I_3) vibrionic emission peak fluorescence intensities were measured and CMC was determined from the inflection point in the plot of log amphiphile concentration and I_3/I_1 ratio.

Measurement of Zeta Potential and Size Distribution

For zeta potential and size distribution analysis, solution of amphiphile was prepared in methanol and dried with nitrogen gas stream at 25°C. The formed film was then hydrated with 10 mL of distilled water to yield a final concentration of ten times the CMC, solution was equilibrated for 24 h at 37°C and 85 rpm. The zeta potential and size distribution of self-assembled micelles were measured by phase analysis light scattering (PALS) and dynamic light scattering (DLS), respectively at 37°C, using Malvern Zetasizer Nanoseries ZS90 (Malvern Instruments Inc, Westborough, USA) equipped with He-Ne laser at 633 nm.

Cell Uptake Studies

Cell uptake studies of FITC loaded micelles were analyzed by confocal microscopy. Suitable aliquots of 2 mg/mL amphiphile stock in methanol were used to bring the final concentration to 10 times above its CMC when suspended in aqueous growth medium. A 1 mL of 2 mg/mL stock solution of FITC was added to the amphiphile and separately to another tube as a free FITC control. Both samples were dried with nitrogen gas stream at 25°C. Samples were then suspended in 10 mL serum free DMEM, vortexed, and equilibrated for 1 h at 37°C and 85 rpm. A2058 melanoma cells seeded on glass coverslips were washed with hank's balanced salt solution (HBSS) followed by serum free medium and incubated with free FITC or FITC loaded micelles at 37°C or 4°C for predetermined time period. Cells were then washed twice with HBSS to remove any unbound micelles or free FITC and incubated with AlexaFluor 594 wheat germ agglutinin to stain cell plasma membranes. These cells were fixed with 4% paraformaldehyde and treated cover slips were mounted on slides and imaged with an inverted Leica DMIRE2 fluorescence microscope (Leica Biosystems Richmond Inc, Richmond, USA) using a Yokogawa CSU-X1 confocal scanner unit.

Average fluorescence intensity of FITC taken up by cells was calculated based on the measurement of 12 individual cells from each treatment group. To maintain consistency, region measurements were based on fixed dimensions of 70×50 (width × height). A t-test was conducted to determine the significance level of FITC internalization within groups treated at 37°C *versus* 4°C, results were considered statistically significant if p value <0.05.

Paclitaxel Loading into Micelles

The paclitaxel loaded micelles were prepared by the solid dispersion method. A 1:1 v/v solution of paclitaxel (1 mg/mL) and amphiphile (10 mg/mL) in methanol was co-dissolved by vortexing followed by shaking in a water bath at 100 rpm and 25°C for 4 h. Methanol was evaporated by passing a nitrogen gas stream. The resulting film was hydrated with 10 mL of distilled water and mixed thoroughly by vortexing. The solution was equilibrated by shaking in the water bath at 25°C and 100 rpm for 12 h. The undissolved drug and excess amphiphile was removed by centrifugation at 16000 rpm for 25 min. The supernatant micellar solution was analyzed for paclitaxel content by HPLC using Waters 2690 Separations Module HPLC system (Waters Corp, Milford, USA) equipped with photodiode array model 996 detector and Phenomenex Gemini C18 column (Phenomenex, Torrance USA) having 250×4.6 mm dimensions. The analysis was performed using gradient elution with water and acetonitrile mixture and increasing the concentration of acetonitrile from 50% to 90%, at time zero to next 10 min and 1 mL/min flow rate. Paclitaxel content was monitored at the wavelength of 227 nm.

Determination of Cytotoxicity

The cytotoxicity study of free paclitaxel and paclitaxel loaded micelles on A2058 melanoma cells and Detroit 551 keratinocyte cells was performed using the SRB colorimetric assay. A2058

melanoma cells or Detroit 551 keratinocyte cells were cultured to 80% confluency in T75 culture flasks using DMEM and EMEM as growth medium, respectively. The cells density was determined using Coulter Counter. The cells were seeded onto 96 well plates at a density of 7000–8000 cells/ well and grown for 24 h to reach 50% confluency. This was followed by treatment with various concentrations of free paclitaxel and paclitaxel loaded micelles ranging from 0.1 to 100 nM for 72 h at 37°C. At the end of the incubation period, the cells were fixed using 10% trichloroacetic acid, followed by washing with distilled water and drying. The cellular proteins were stained using 50 μL of 0.4% SRB in 1% acetic acid. Unbound SRB was washed with 1% acetic acid and the plates were dried overnight. The cell bound SRB was then solubilized using 200 μL of 10 mM unbuffered Tris base solution. SRB absorbance was measured at 560 nm wavelength using a TriStar LB 941 Plate Reader (Berthold Technology, Oak Ridge, USA). The percentage viability of cells was plotted as a function of log paclitaxel concentration and data was analysed in Graph Pad Prism Version 5.0d software (GraphPad Software Inc, CA, USA) using nonlinear-regression curve fit (variable slope four parameter equation).

In Vitro Stability Using FRET Analysis

The *in vitro* stability of micelles was assessed using FRET method. FRET pair, DiI and DiO were loaded into micelles by dissolving in DMF (at a concentration of 2.5 mM each) and mixing with a solution of amphiphile in DMF at concentration of 30 times over CMC. Further, the solution was heated at 50°C on a water bath for 5–6 h, followed by dialysis through a 1000 kDa membrane. The dialysis was performed for 24 h and water in the bath was exchanged with fresh water three times in this duration. The FRET pair loaded micelles were diluted 10 fold (three times above CMC) and 30 fold (at CMC) in water and in acetone. Fluorescence spectra were recorded at excitation wavelength of 484 nm and emission wavelength range of 495 to 600 nm. The FRET efficiency was obtained from the ratio $I_{565}/(I_{565} + I_{501})$. Further, time resolved spectra were obtained after 10 fold dilution of micelles in water. Using the same procedure, DiO loaded micelles and DiI loaded micelles were prepared and diluted with water in the ratio 1:1:8 and time resolved spectra were measured.

RESULTS

Peptide Amphiphiles Synthesis

Four amphiphiles (shown in Fig. 1) with one or two units of ADA linker having either C16 or C18 fatty acid were synthesized. The synthesis of the amphiphiles was carried as shown in the schematic (Fig. 2) by solid phase peptide synthesis on Wang resin using standard Fmoc chemistry (30). In the first phase of synthesis, RGD peptide was extended on preloaded aspartic acid, followed by conjugation of one or two units ADA linker to amino group of arginine. Finally, the C16 or C18 fatty acid was added to NH_2 terminus of group of ADA linker. Data from mass spectroscopy, H^1NMR and HPLC confirmed the formation of PAs along with corresponding high purity. As an example, the yield of C18-$(ADA)_2$-RGD amphiphile was 38%, purity determined by HPLC was 93.62%, confirmed mass was 903.6. The ^{1}H NMR spectra of this amphiphile in DMSO-d_6, at 600 MHz showed δ 0.80–0.82 (t, $\mathcal{J}$=6.7 and 7.2 Hz,3H), 1.19 (s, 30H), 1.39–1.47 (m, 4H), 1.50–1.56 (m, 1H), 1.65–1.71 (m, 1H), 1.99–2.02 (t, $\mathcal{J}$=7.3 and 7.4 Hz, 2H), 2.53–2.57 (dd, $\mathcal{J}$=6.8, 9.8 and 6.7 Hz, 1H), 2.62–2.66 (dd, $\mathcal{J}$=5.7, 10.9 and 5.6 Hz, 1H), 3.03–3.07 (q, $\mathcal{J}$=6.9 and 6.3 Hz, 2H), 3.13–3.16 (q, $\mathcal{J}$=5.8 and 6 Hz, 2H), 3.20–3.29 (m, 2H), 3.35–3.37 (t, $\mathcal{J}$=6 Hz, 2H), 3.40–3.42 (t, $\mathcal{J}$=6.1 and 6 Hz, 2H), 3.49–3.59 (m, 8H), 3.71–3.72 (d, $\mathcal{J}$=6.9 Hz, 2H), 3.83 (s, 2H), 3.89 (d, $\mathcal{J}$=2.7 Hz, 2H), 4.32–4.35 (q, $\mathcal{J}$=7.8, 5.8 and 8.0 Hz, 1H), 4.48–4.52 (q, $\mathcal{J}$=6.7, 7.3 and 6.5 Hz, 1H), 7.40–7.41 (t, $\mathcal{J}$=5.6 and 5.7 Hz, 1H), 7.65–7.68 (q, $\mathcal{J}$= 5.8, 7.3 and 8.2 Hz, 2H), 7.78–7.80 (t, $\mathcal{J}$=6.0 and 5.4 Hz, 1H), 8.20–8.21 (d, $\mathcal{J}$=7.8 Hz, 1H), 8.30–8.32 (t, $\mathcal{J}$=5.8 Hz, 1H) confirming the formation. The mass spectrum and ^{1}H NMR spectrum of C18-$(ADA)_2$-RGD amphiphile is shown in Figs. 3 and 4, respectively. Similarly, mass spectra and ^{1}H NMR spectral analysis of other compounds also confirmed their formation.

Critical Micellar Concentration, Size and Zeta Potential Determination

The CMC data with fluorescence spectroscopy technique using pyrene as probe indicated that all amphiphiles self-assembled into micelles. Pyrene is a polycyclic aromatic hydrocarbon, widely used for determination of CMC because of its monomer fluorescence spectra exhibits distinct vibrational bands (31,32). The intensities of these vibrational bands depend upon solvent environment around pyrene monomers, which is influenced by both dipole moment and dielectric constant of solvent (33). As shown in the excitation spectra of pyrene in various concentration of C18-$(ADA)_2$-RGD (Fig. 5), below CMC the ratio of I_3/I_1 is low due to the pyrene surrounded by aqueous environment. Conversely, an increase in the concentration of amphiphile leads to micelle formation, which is driven by the hydrophobic collapse of long alkyl chains. During this self-assembly, pyrene partitions into the hydrophobic core of micelles, resulting in a high I_3/I_1 fluorescence ratio. The intersection point of the flat line drawn through the concentrations below CMC and another sharply rising line drawn

Fig. 1 Molecular structures of synthesized peptide amphiphiles.

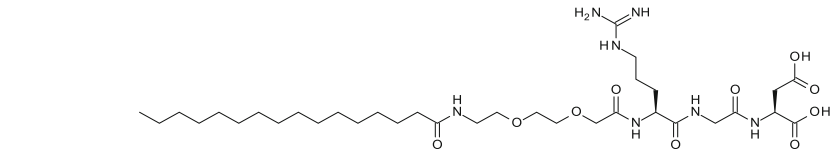

C16-(ADA)-RGD

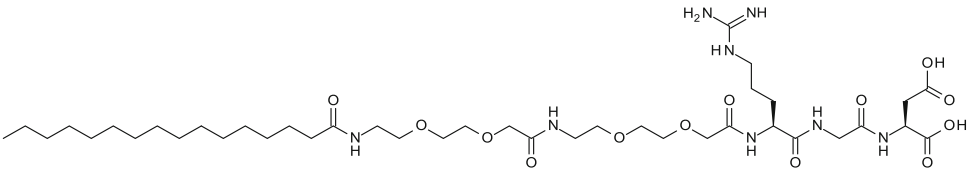

C16-(ADA)$_2$-RGD

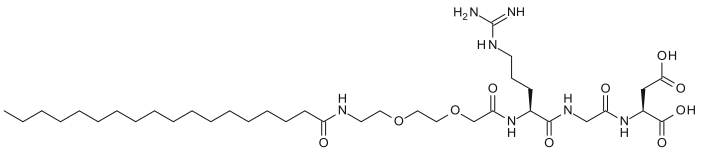

C18-ADA-RGD

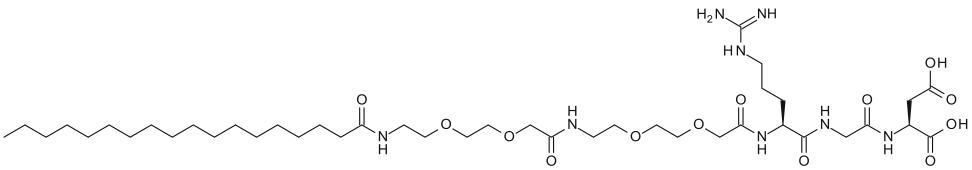

C18-(ADA)$_2$-RGD

through the concentrations above CMC, represents CMC value. The CMC values of amphiphiles determined with fluorescence spectroscopy method are shown in Table I. It is evident that CMC values of amphiphiles decreased significantly by increasing the fatty acid chain length from C16 to C18. In contrast, increase in number of ADA units did not significantly impact CMC.

Hydrodynamic diameter measurements using DLS analysis indicated that amphiphiles self-assembled to form micelles with unimodal distribution, a representative size distribution chart of C18-(ADA)$_2$-RGD micelles is given in Fig. 6. The size of micelles increased with increase in alkyl chain length from C16 to C18, whereas variation in the number of ADA units did not exhibit any discernible trend. Correspondingly, ADA incorporation in both C16 and C18 series brought down micelles size to favourable targeting size range of 20–200 nm (34), when compared to C16-RGD and C18-RGD micelles. Similarly, the zeta potential measurements with PALS method revealed that incorporation of ADA and increase of ADA units in amphiphile structure decreased negative zeta potential of micelles to near zero in C18 series and to high positive zeta potential in C16 series, in contrast with negative zeta potential of C18-RGD micelles and C16-RGD micelles (Table I). The C18-(ADA)$_2$-RGD micelles were chosen for cellular uptake, cytotoxicity and kinetic stability studies because of their lower CMC, smaller size and near zero zeta potential (35,36).

Cellular Uptake of C18-(ADA)$_2$-RGD Micelles

FITC was loaded into C18-(ADA)$_2$-RGD micelles by hydrating the co-dispersed film of FITC and C18-(ADA)$_2$-RGD amphiphile with serum free cell culture medium. Hydrodynamic diameter of these micelles was analysed by DLS method as described above and it was found to be

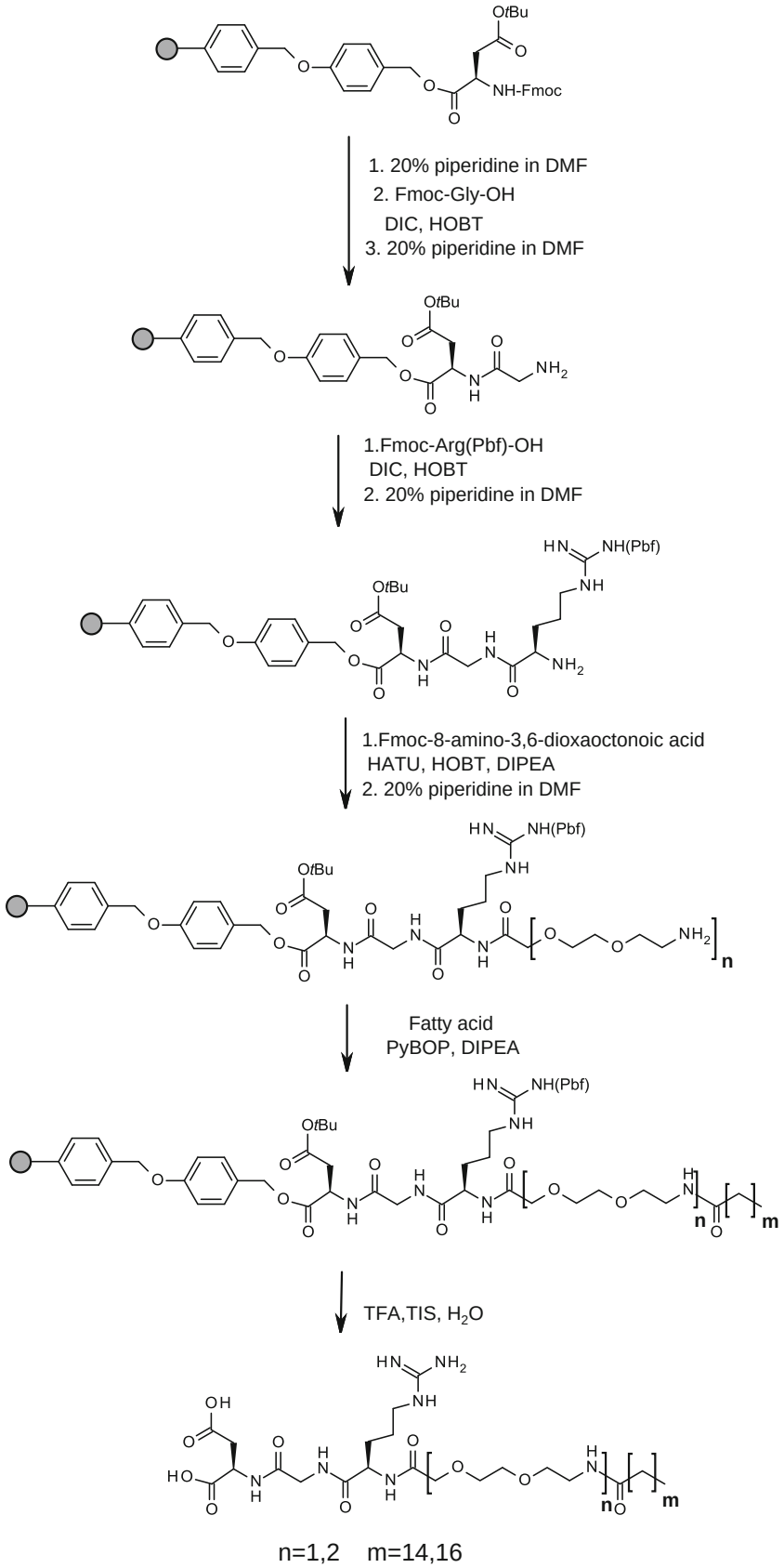

Fig. 2 Schematic representation of the solid phase synthesis of peptide amphiphiles.

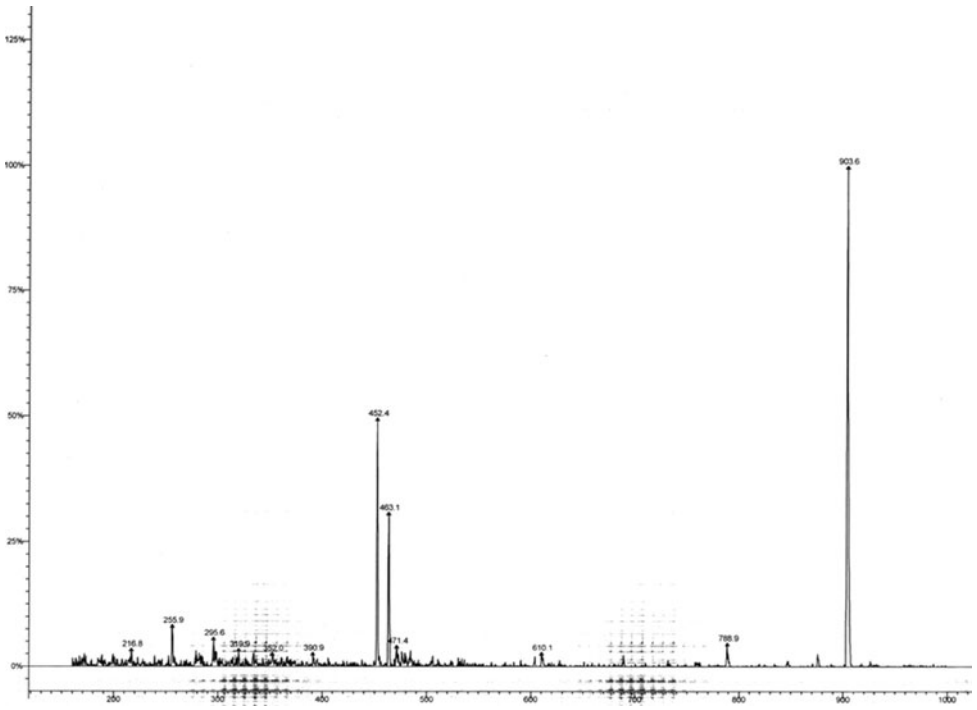

Fig. 3 Mass spectrum of C18-$(ADA)_2$-RGD amphiphile.

133.13 ± 7.64 nm. In preliminary experiments, A2058 melanoma cells were incubated with FITC loaded C18-$(ADA)_2$-RGD micelles at 2, 5, and 10 min time points to determine binding and optimal internalization periods. Results from these studies suggested that maximum uptake was seen at a 10 min treatment period.

Subsequent studies were aimed to determining the mechanism by which FITC loaded C18-$(ADA)_2$-RGD micelles internalize in A2058 melanoma cells. This was carried out by performing temperature dependent studies in which A2058 melanoma cells were incubated at 4°C and 37°C for 10 min. Confocal microscopy images of FITC loaded

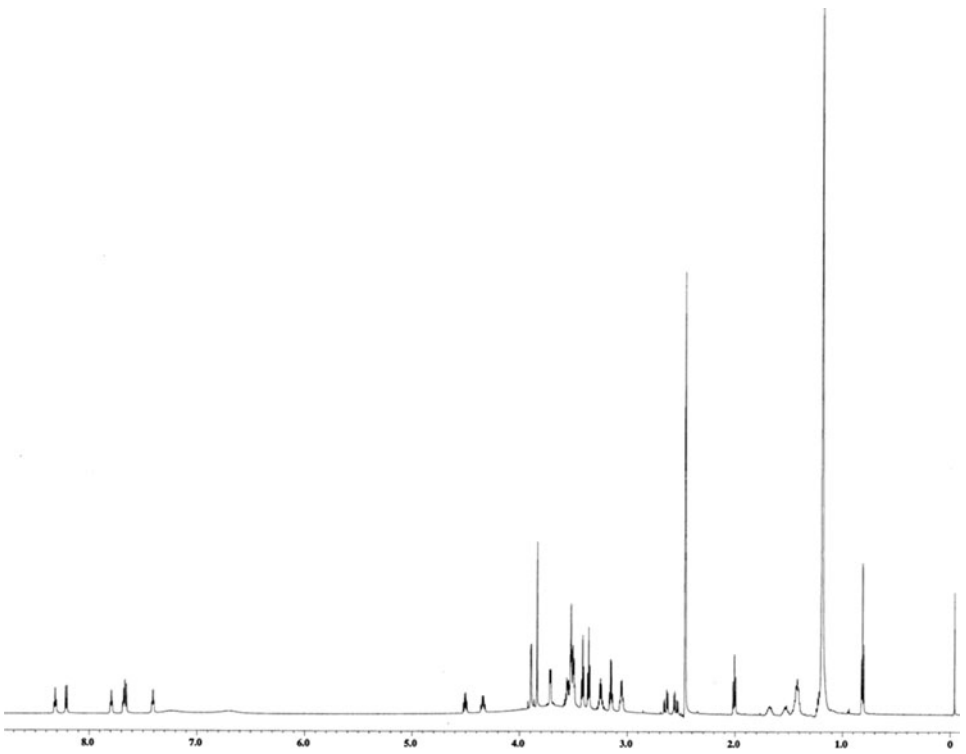

Fig. 4 ^1H NMR spectrum of C18-$(ADA)_2$-RGD amphiphile in DMSO-d_6.

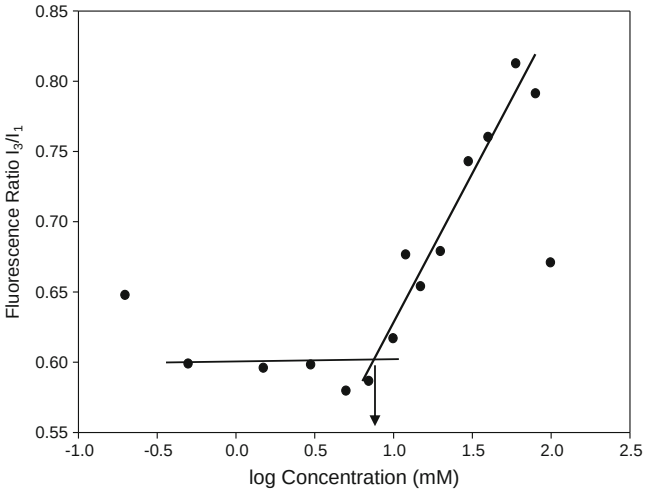

Fig. 5 Fluorescence spectra of C18-$(ADA)_2$-RGD amphiphile showing CMC ($n=3$).

C18-$(ADA)_2$-RGD micelle internalization in melanoma cells are shown in Fig. 7. At 37°C, A2058 melanoma cells incubated with C18-$(ADA)_2$-RGD micelles showed marked cellular uptake of FITC when compared to cells incubated with free FITC (Fig. 7a and b). Reducing the incubation temperature to 4°C significantly decreased cellular uptake of FITC loaded C18-$(ADA)_2$-RGD micelles by A2058 melanoma cells (Fig. 7a and c). In difference, there was no appreciable variance in cellular uptake of FITC into A2058 melanoma cells treated with free FITC either at 37°C or 4°C incubation temperature (Fig. 7b and d). The small molecular weight of free FITC can account for minor amount of its internalization in cells by passive diffusion. It is evident from confocal microscopy images that the intracellular uptake of FITC was increased not only when delivered through C18-$(ADA)_2$-RGD micelles, but also when driven by an energy dependent mechanism, which can only occur when the cells are subjected to the metabolically active temperature of 37°C.

The fluorescence intensity from confocal microscopy analysis was quantified and the data is shown in Fig. 8. A 3 fold increase in average intracellular fluorescence intensity when A2058 melanoma cells were treated with micelles at 37°C when compared to cells treated with free FITC at the same temperature ($p<0.05$). Importantly, C18-$(ADA)_2$-RGD micelles also showed significant intracellular uptake of FITC when treated at 37°C *versus* 4°C ($p<0.05$). There was not a significant difference in average fluorescence intensity in A2058 melanoma cells incubated with either FITC loaded C18-$(ADA)_2$-RGD micelles or free FITC at 4°C. Collectively, the data suggested that C18-$(ADA)_2$-RGD micelles can efficiently deliver entrapped hydrophobic agents to cancer cells by an active process. Our data is consistent with reported role of receptor mediated endocytosis in the uptake of RGD micelles, and based on the temperature dependent analysis (37).

Table I Characterization of Amphiphiles and Self-Assembled Micelles

Amphiphile	CMC value(μM)	Size (nm)	Zeta Potential (mV)
C16-RGD	60.67 ± 0.58	266.5 ± 1.6	−39.6 ± 0.2
C16- ADA-RGD	30.07 ± 0.12	149.87 ± 25.91	−0.80 ± 2.24
C16-$(ADA)_2$-RGD	30.07 ± 0.12	96.09 ± 8.33	9.50 ± 0.89
C18-RGD	43.43 ± 1.01	450.2 ± 65.3	−13.5 ± 10.2
C18- ADA-RGD	13.17 ± 0.76	179.00 ± 13.41	−2.62 ± 0.74
C18-$(ADA)_2$-RGD	9.00 ± 1.73	194.63 ± 44.86	0.27 ± 1.96

Paclitaxel Loaded C18-$(ADA)_2$-RGD Micelles Cytotoxicity Studies

Solid dispersion method was adopted to load paclitaxel into C18-$(ADA)_2$-RGD micelles using methanol as organic medium. HPLC analysis for determination of paclitaxel content in C18-$(ADA)_2$-RGD micelles revealed an increase in the paclitaxel aqueous solubility from 0.4 μg/mL to 9.05 μg/mL. To determine cytotoxicity of free paclitaxel and paclitaxel loaded in C18-$(ADA)_2$-RGD micelles in $\alpha_v\beta_3$ integrin overexpressing A2058 melanoma cells and normal Detroit 551 keratinocyte cells, different concentrations of paclitaxel and paclitaxel loaded C18-$(ADA)_2$-RGD micelles were incubated with these cell lines for 72 h and cell viability was measured with SRB assay. IC50, which the concentration of drug required to achieve 50% inhibition of cell proliferation, was measured. The IC50 values calculated using the hill slope obtained from the cytotoxicity profiles of free paclitaxel and paclitaxel micellar formulation, confirmed the specific role of $\alpha_v\beta_3$ integrin in the uptake of these paclitaxel loaded micelles. In $\alpha_v\beta_3$ integrin overexpressing A2058 melanoma cells, IC50 value of paclitaxel decreased from 7.85×10^{-3} μM (for free paclitaxel) to 4.70×10^{-3} μM when loaded in C18-$(ADA)_2$-RGD micelles (Fig. 9a and b). In the normal cell line, Detroit 551 keratinocyte cells, IC50 value of paclitaxel increased from 4.77×10^{-3} μM (for free paclitaxel) to 22.53×10^{-3} μM when loaded in C18-$(ADA)_2$-RGD micelles (Fig. 9c and d). The results of the cytotoxicity studies further elicit the specific role of $\alpha_v\beta_3$ integrin in the cellular uptake of the micelles.

In Vitro Stability Using FRET Analysis

The DiO+DiI loaded C18-$(ADA)_2$-RGD micelles exhibited emission maximum around 565 nm when undiluted and also upon 10 fold dilution with water. This spectrum was obtained due to the close proximity of the FRET dyes loaded in the hydrophobic core of the micelles, which enabled fluorescence quenching (Fig. 10). Dilution in organic

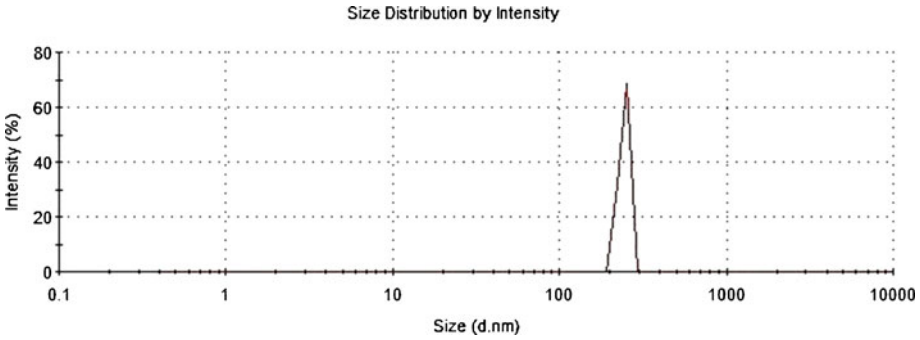

Fig. 6 Size distribution of C18-$(ADA)_2$-RGD micelles in aqueous medium by DLS method.

solvent resulted in the disruption of self-assembly structures (micelles) solubilizing the dye and shifted the peak to 501 nm. The FRET efficiency was found to be 0.99 on 10 fold dilution in water and it decreased to 0.19 on dilution in acetone. Even upon 30 fold dilution in water, a high FRET efficiency of 0.96 was observed. From this data it was clear that the dyes were loaded inside strong micellar core as opposed to presence of any loose aggregates on dilution in water. Further, when the DiI+DiO loaded C18-$(ADA)_2$-RGD micelles were diluted in water and emission spectrum was recorded over a period of 24 h, no significant change in the FRET efficiency over time was observed (Fig. 11). To confirm the kinetic stability of the micelles, the dyes were also loaded individually in the C18-$(ADA)_2$-RGD amphiphiles and then diluted up to 10 fold in water. The leakage of the dyes from the micellar core and exchange between individual micelles was assessed from the increase in FRET efficiency over time. The observed FRET efficiency increased by approximately 12% over 24 h (Fig. 12). The C16-RGD and C18-RGD micelles without ADA linker were loaded with the dyes, however, the micelles formed aggregates with low dye incorporation. This observation is similar to the hydrophobic interactions found in the size and drug loading characterizations.

DISCUSSION

Fatty acid conjugation to peptides is a known strategy in the field of peptide therapeutics. Such approaches have been employed to stabilize the secondary structure of peptides, enhance biological activity, better membrane permeability

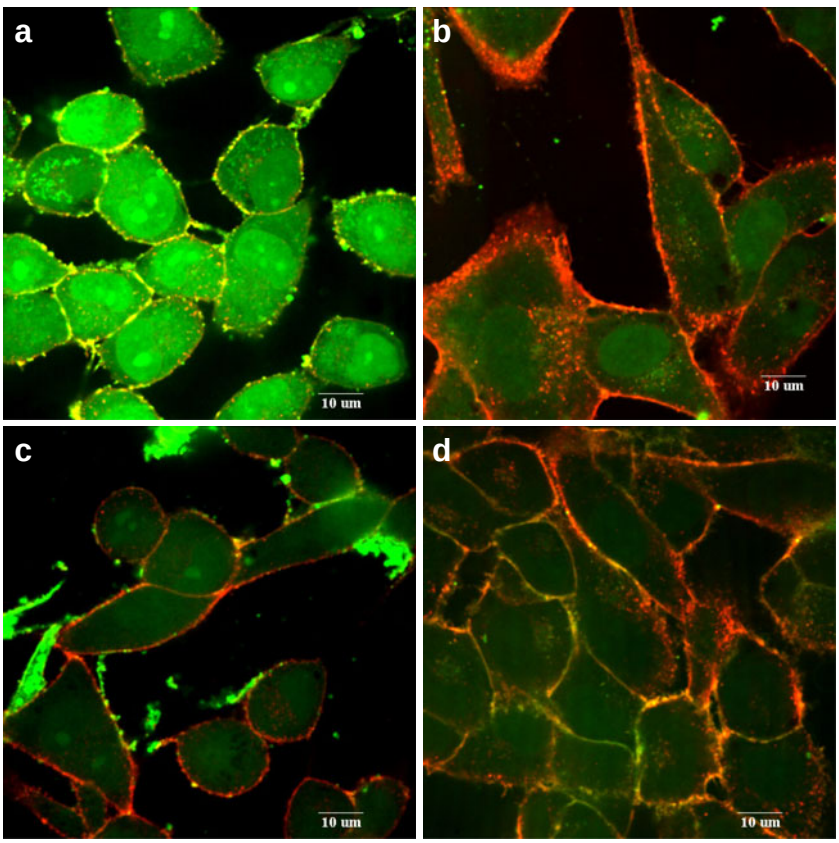

Fig. 7 Confocal microscopy images of A2058 melanoma cells incubated for 10 min, at 37°C with FITC loaded C18-$(ADA)_2$-RGD micelles (**a**), at 37°C with free FITC (**b**), at 4°C with FITC loaded C18-$(ADA)_2$-RGD micelles (**c**), and at 4°C with free FITC (**d**).

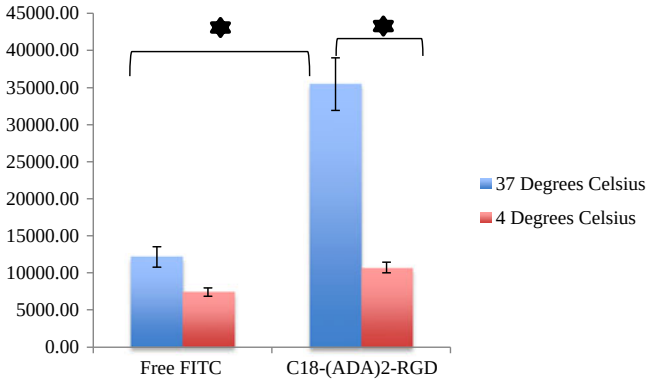

Fig. 8 Cellular uptake of free FITC and FITC loaded C18-$(ADA)_2$-RGD micelles after 10 min incubation time period at 4°C and 37°C. Each bar represents average fluorescence intensity in A2058 melanoma cells ± SD after 10 min of incubation time period ($n=12$). Statistical analysis between groups was performed by t-test (*$p<0.05$).

and improve pharmacokinetics profile (38–40). Amphiphilic nature of fatty acid conjugated peptide can be utilized in drug delivery as they self-assemble in aqueous environment to encapsulate the hydrophobic drugs in their nanostructures. If nanostructure are designed to have ligands on their surface to interact with a particular biological target, their potential as drug carriers for the active targeted drug delivery significantly improves. Recent reports pertaining to development of PAs nanostructures for drug delivery applications are emerging from many research groups (41,42). In this report, four amphiphiles of C16 and C18 fatty acid-RGD peptide amphiphiles with either one or two units of ADA linker were designed and synthesized to target $\alpha_v\beta_3$ integrin overexpressing tumor cells. These amphiphiles were designed to have three segments, polar RGD peptide segment for the binding of $\alpha_v\beta_3$ integrin, ADA hydrophilic linker, and C16 or C18 aliphatic acid. Several peptide sequences containing the RGD motifs with improved or reduced affinity have been discovered for $\alpha_v\beta_3$ integrin binding, however tripeptide RGD has important contacts and suffices for use as a targeting ligand (43). ADA hydrophilic linker was incorporated in between RGD and long alkyl chain interface to overcome excess hydrophobicity of previous amphiphiles. C16 and C18 long alkyl chains were used as hydrophobic segment to aid in self-assembly. In the designing, emphasis was given to optimal hydrophobicity because too much hydrophobicity causes toxicity to cells, difficult to solubilize them in aqueous media used in their evaluation, and leads to non-specific binding to the cell membranes. Initially, PAs synthesis was carried out by synthesizing RGD peptide on Wang resin and pentafluorophenyl ester of C16 or C18 - ADA acid with the reported procedure (44) separately. Eventually, both precursors were conjugated in solid phase synthesis. The purity of the amphiphiles obtained from this procedure was very low, possible reason for the low purity is degradation of pentafluorophenyl ester precursor in reaction conditions. So, the entire amphiphile was synthesized in solid phase by the chain elongation. Several coupling agents

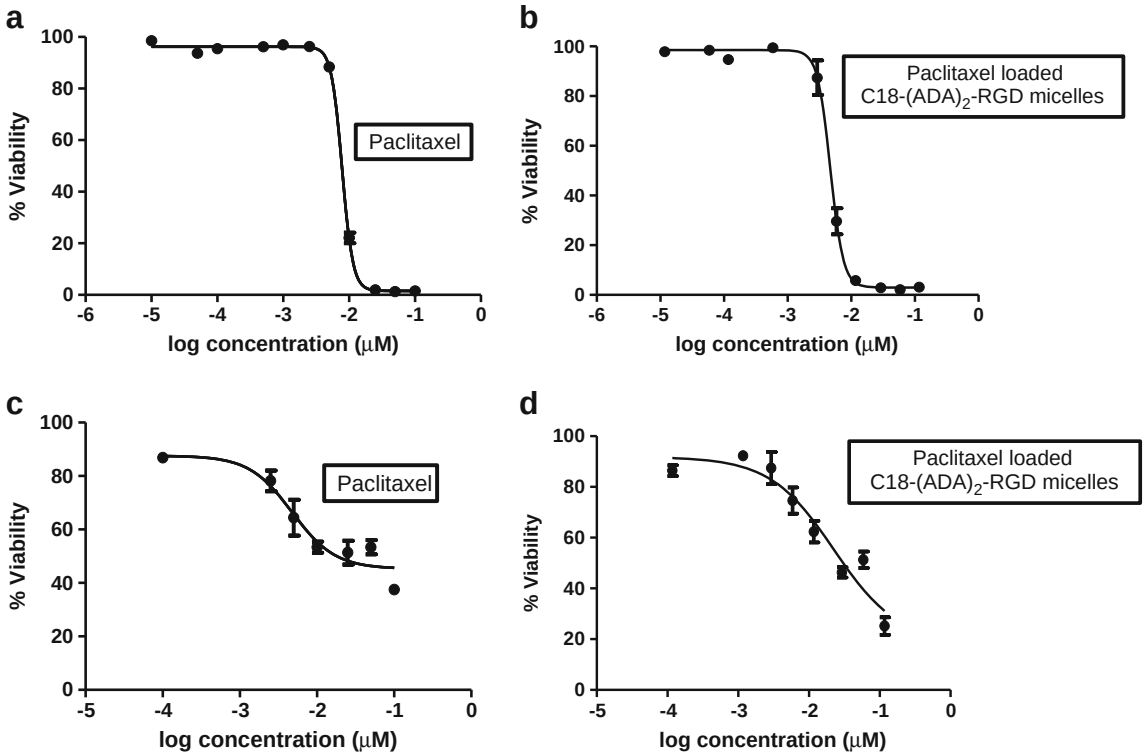

Fig. 9 IC50 of paclitaxel and paclitaxel loaded C18-$(ADA)_2$-RGD micelles in A2058 melanoma cells (**a**) and (**b**), in Detroit 551 keratinocyte cells after 72 h treatment (**c**) and (**d**) after 72 h treatment ($n=3$).

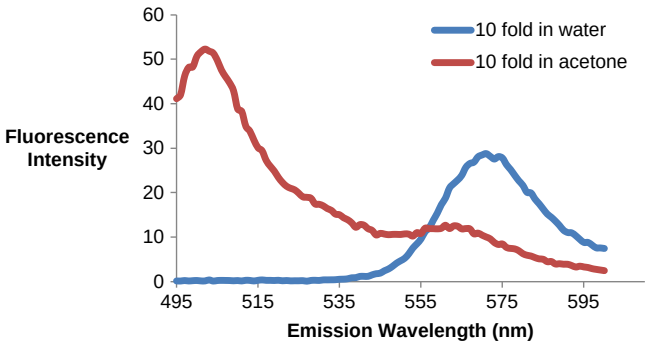

Fig. 10 Emission spectra of DiI+DiO loaded C18-$(ADA)_2$-RGD micelles diluted 10 fold in water and 10 fold in acetone. The concentration of amphiphiles on 10 fold dilution is 3 times above CMC.

were screened to optimize coupling of ADA linker and fatty acids. Of these, HATU and PyBOP were found to be suitable coupling agents for the coupling of ADA linker and fatty acids, respectively. C18 amphiphiles have shown higher retention time in HPLC analysis than C16 amphiphiles, demonstrating higher hydrophobicity for C18 amphiphiles. The molecular weight of the amphiphiles determined through mass spectroscopy, are in good agreement with calculated molecular weights. Peak assignment for ^{1}H NMR spectrum confirmed distinctive peaks attributed to RGD, ADA and fatty acid segments.

The four amphiphiles synthesized have self-assembled at micro molar range concentration. These amphiphiles self-assembled at 100 times lower CMC values than that of low molecular surfactants, that have typical CMC range of 10^3–10^4 M (45). The low CMC values are indicative of high stability of self-assembled nanostructures upon dilution in physiological fluids, and longer circulation time. Increase in the chain length from C16 to C18 considerably decreased CMC, while there was no significant change in the CMC when number of ADA linker units increased. Modification of block copolymers in the length of hydrophilic block had no significant effect on CMC, because thermodynamic parameters of micellization such as entropy, enthalpy and free energy are not affected by these modifications and the current amphiphiles confirmed that (46). The lower CMC values also suggest that the hydrophobic tails of PAs are self-assembled with strong Van der Waals interactions forming the core of micelles. This enables tight encapsulation and prevents the leakage of hydrophobic molecules from micelles, maximizing the amount of loaded drug cargo to the site of action (47), and among the amphiphiles C18-$(ADA)_2$-RGD showed lowest CMC. Size and zeta potential of the micelles are important factors in determining the outcome of their behaviour in biological system. Smaller size micelles (5–10 nm) are eliminated through the kidney, while larger micelles (>600 nm) may not cross the tumor vasculature (48). The C18-ADA_2-RGD exhibited the lowest CMC amongst all the amphiphiles, which was the main criteria for its selection. The C18-ADA_2-RGD micelles had a zetapotential of 0.27 mV, that could improve pharmacokinetics by suppressing plasma protein adsorption and minimizing nonspecific cellular uptake (49,50). Though

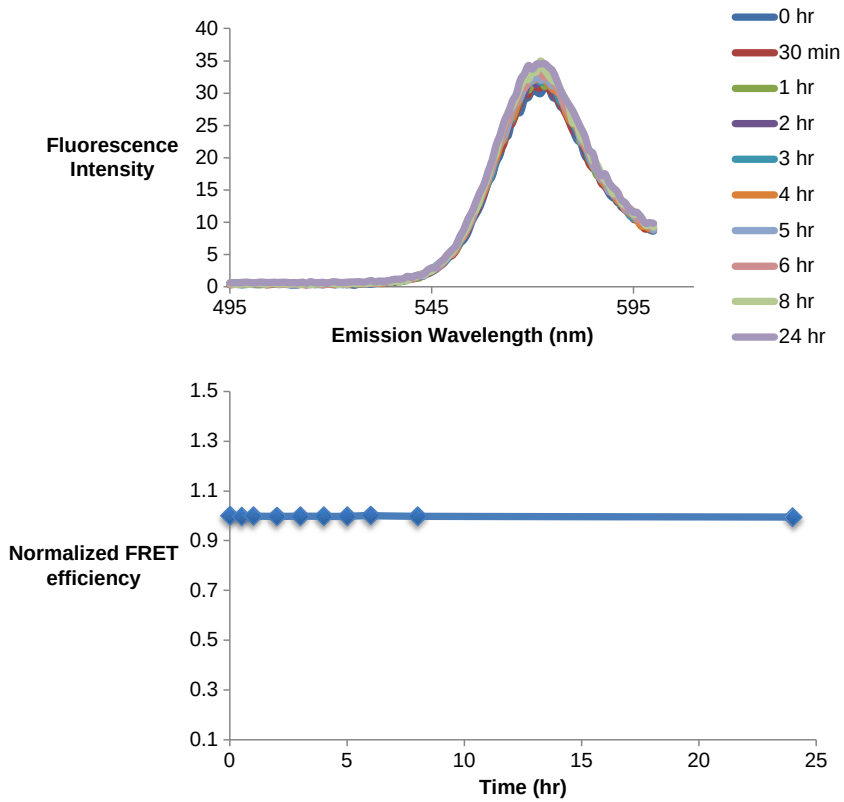

Fig. 11 Time resolved emission spectra of DiO+DiI loaded C18-$(ADA)_2$-RGD micelles diluted 10 fold in water (n=3).

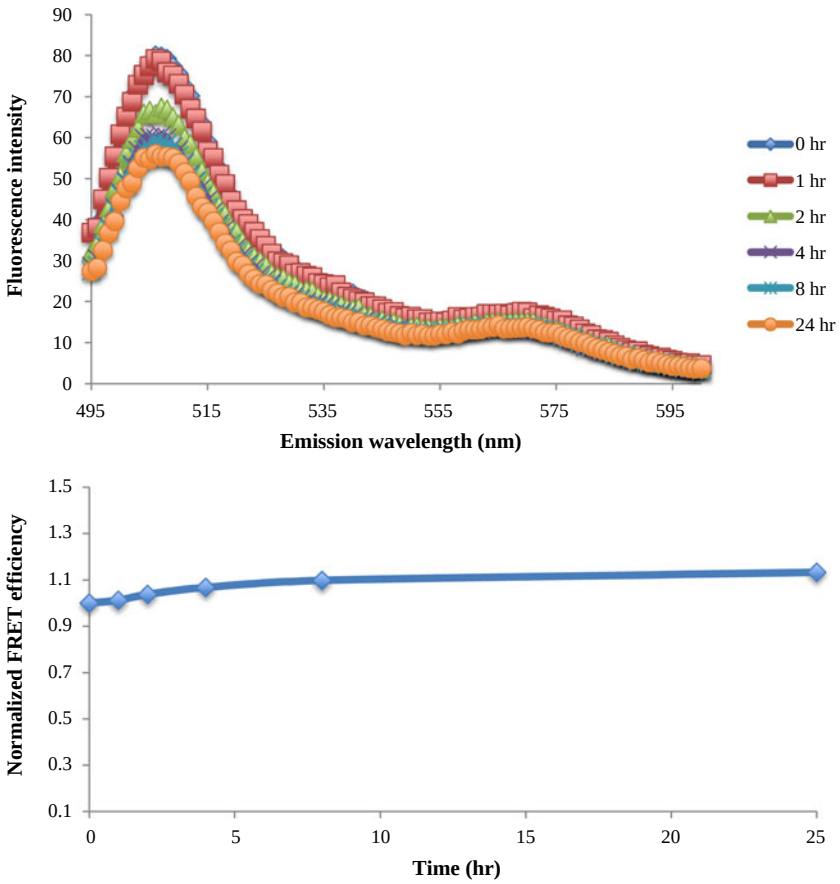

Fig. 12 Time resolved emission spectra of separate DiO loaded C18-$(ADA)_2$-RGD micelles and DiI loaded C18-$(ADA)_2$-RGD micelles, mixed and diluted up to 10 fold in water (n=3).

C16-$(ADA)_2$-RGD micelles exhibited suitable size, their CMC and positive zeta potential are higher and could cause short plasma half-life due to dissociation upon dilution and interactions with blood components (36). Based on the lower CMC, size and zeta potential analysis C18-$(ADA)_2$-RGD micelles were further characterized for cellular uptake, cytotoxicity and kinetic stability studies.

FITC was used as fluorescence probe for cellular uptake studies in A2058 melanoma cells due to lack of intrinsic fluorescence property for paclitaxel. In addition, the moderate hydrophobicity of this probe served as a model cargo for cellular uptake studies in both its free and encapsulated form. Both qualitative and quantitative cellular uptake studies of FITC loaded C18-$(ADA)_2$-RGD micelles using confocal microscopy showed enhanced fluorescence in the cells incubated with FITC loaded C18-$(ADA)_2$-RGD micelles at 37°C in comparison of cells incubated with free FITC at 10 min time points. The amount of fluorescence intensity was 65% higher in the cells incubated with FITC loaded C18-$(ADA)_2$-RGD micelles. The maximum uptake in short duration suggested fast uptake and delivery of FITC loaded in C18-$(ADA)_2$-RGD micelles into the cells, and these results are similar to previously reported findings of Castel *et al.* with cyclo-RGDfK-carboxyfluorescein (51). To prove energy dependent uptake mechanisms, similar experiments were conducted at 4°C incubation temperature. There was 70% reduction in the fluorescence intensity in the cells incubated with FITC loaded C18-$(ADA)_2$-RGD micelles in comparison of 37°C incubation temperature. This data suggested that cellular uptake of FITC loaded C18-$(ADA)_2$-RGD micelles is driven by energy dependent mechanism. The amount of fluorescence in cells incubated with free FITC at both 4°C and 37°C temperature is lower than the micellar treated cells, indicating some FITC diffused across the cell membrane by passive diffusion. Poorly soluble anticancer agent, paclitaxel, was loaded into C18-$(ADA)_2$-RGD micelles by solid dispersion technique, in order to assess the utility of these peptide amphiphiles as carriers for targeted delivery of hydrophobic anticancer drugs to tumor endothelium. The micelles have anisotropic distribution of water molecules, which means that there is decrease in concentration of water from shell to core (52). Owing to this difference in polarity in the various regions of the micelle, the aqueous solubility of paclitaxel was increased by 20 folds, which is attributed to entrapment of the hydrophobic drug into the hydrophobic core of micelles during self-assembly. Cytotoxicity of free paclitaxel and paclitaxel loaded into C18-$(ADA)_2$-RGD micelles was determined in two cell lines that had different levels of $\alpha_v\beta_3$ integrin expression. In A2058 melanoma cells that have higher $\alpha_v\beta_3$ integrin expression, C18-$(ADA)_2$-RGD micelles containing paclitaxel showed

IC50 value that is almost half in comparison to free drug. This decrease in the IC50 value in the $\alpha_v\beta_3$ integrin overexpressing cells indicated that RGD decorated micelles can target to these cells. On the other hand, a four fold increase in the IC50 value observed in the Detroit 551 keratinocyte cells when compared to A2058 melanoma cells showed the specificity of these RGD carriers towards $\alpha_v\beta_3$ integrin overexpressing cells.

FRET is an excellent tool for the determination of stability of micelles and the stability kinetics of the C18-$(ADA)_2$-RGD micelles on dilution with water, was studied using this method. FRET pairs exhibit different emission spectra based on the distance between the individual FRET dye molecules (53,54). The DiI+DiO loaded micelles exhibited a high FRET efficiency even on dilution in water up to 30 fold due to close proximity of the dyes in the micelle core. Alternatively, upon dilution in acetone, the energy transfer disappeared and FRET efficiency decreased significantly due to escape of the dye molecules from the core. The micelles upon 10 fold dilution in water were stable when observed up to 24 h and did not disassemble as seen from the nearly constant FRET efficiency over the time. To support this data further, the DiI and DiO were also individually loaded into the micelles and the diluted in water to determine the dye exchange between micelles. Since the dyes are hydrophobic, upon leakage from the micelle, they might partition into the hydrophobic core of another micelle. The FRET efficiency from these micelles increased by 12% over a 24 h period, suggesting a low dye exchange between the micelles, in spite of the system not being highly cross-linked (55). These studies revealed that the micelles showed good kinetic stability upon several fold dilution. C18-RGD and C16-RGD micelles exhibited a low dye loading and hence could not be analyzed further for comparison purposes, indicating hydrophilic linker such as ADA is essential for the accurate characterization of micelles.

CONCLUSION

Amphiphiles of fatty acid- RGD with ADA linker having improved hydrophilicity were designed and synthesized for active targeted delivery of paclitaxel. The amphiphiles were characterized for their micelle forming properties and specific uptake by $\alpha_v\beta_3$ integrin expressing cells. Lower CMC values of PAs containing the ADA linker may contribute to their improved kinetic stability *in vivo* (56). Incorporation of ADA linker between interface of RGD peptide and fatty acid reduced the size and zeta potential of micelles. The CMC, size and zeta potential analysis results proposed that C18-$(ADA)_2$-RGD micelles were found to be suitable for further investigation. FITC loaded C18-$(ADA)_2$-RGD micelles were taken up by $\alpha_v\beta_3$ integrin expressing cells through energy dependent mechanism. The cytotoxicity evaluation revealed specific role of $\alpha_v\beta_3$ integrin in the uptake of these carriers. The FRET studies revealed the kinetic stability of the micelles. The dye loaded micellar core was intact upon dilution with water and exchange of molecules between micellar cores was low. In conclusion, the feasibility of synthesis and characterization of fatty acid-RGD micelles with ADA linker for active targeting of hydrophobic drugs to $\alpha_v\beta_3$ integrin expressing cells was demonstrated.

REFERENCES

1. Shimada T, Lee S, Bates FS, Hotta A, Tirrel M. Wormlike micelle formation in peptide-lipid conjugates driven by secondary structure transformation of the headgroups. J Phys Chem B. 2009;113 (42):13711–4.
2. Rexeisen EL, Fan W, Pangburn TO, Taribagil RR, Bates FS, Lodge TP, *et al.* Self-assembly of fibronectin mimetic peptide-amphiphile nanofibers. Langmuir. 2010;26(3):1953–9.
3. Pashuck ET, Stupp SI. Direct observation of morphological transformation from twisted ribbons into helical ribbons. J Am Chem Soc. 2010;132(26):8819–21.
4. Ziserman L, Lee HY, Raghavan SR, Mor A, Danino D. Unraveling the mechanism of nanotube formation by chiral self-assembly of amphiphiles. J Am Chem Soc. 2011;133(8):2511–7.
5. Cui H, Muraoka T, Cheetham AG, Stupp SI. Self-assembly of giant peptide nanobelts. Nano Lett. 2009;9(3):945–51.
6. Niece KL, Hartgerink JD, Donners JJJM, Stupp SI. Self-assembly combining two bioactive peptide-amphiphile molecules into nanofibers by electrostatic attraction. J Am Chem Soc. 2003;125 (24):7146–7.
7. Han S, Cao S, Wang Y, Wang J, Xia D, Xu H, *et al.* Self-Assembly of short peptide amphiphiles: the cooperative effect of hydrophobic interaction and hydrogen bonding. Chem Eur J. 2011;17 (46):13095–102.
8. Xu XD, Jin Y, Liu Y, Zhang XZ, Zhuo RX. Self-assembly behavior of peptide amphiphiles (PAs) with different length of hydrophobic alkyl tails. Colloids Surf B Biointerfaces. 2010;81(1):329–35.
9. Webber MJ, Tongers J, Renault MA, Roncalli JG, Losordo DW, Stupp SI. Development of bioactive peptide amphiphiles for therapeutic cell delivery. Acta Biomater. 2010;6(1):3–11.
10. Angeloni NL, Bond CW, Tang Y, Harrington DA, Zhang S, Stupp SI, *et al.* Regeneration of the cavernous nerve by sonic hedgehog using aligned peptide amphiphile nanofibers. Biomaterials. 2011;32(4):1091–101.
11. Chow LW, Wang LJ, Kaufman DB, Stupp SI. Self-assembling nanostructures to deliver angiogenic factors to pancreatic islets. Biomaterials. 2010;31(24):6154–61.
12. Bulut S, Erkal TS, Toksoz S, Tekinay AB, Tekinay T, Guler MO. Slow release and delivery of antisense oligonucleotide drug by self-assembled peptide amphiphile nanofibers. Biomacromolecules. 2011;12(8):3007–14.
13. Wiradharma N, Tong YW, Yang YY. Self-assembled oligopeptide nanostructures for co-delivery of drug and gene with synergistic therapeutic effect. Biomaterials. 2009;30(17):3100–9.
14. Guler MO, Claussen RC, Stupp SI. Encapsulation of pyrene within self-assembled peptide amphiphile nanofibers. J Mater Chem. 2005;15(42):4507–12.
15. Chen JX, Wang HY, Li C, Han K, Zhang XZ, Zhuo RX. Construction of surfactant-like tetra-tail amphiphilic peptide with RGD ligand for encapsulation of porphyrin for photodynamic therapy. Biomaterials. 2011;32(6):1678–84.

16. Accardo A, Tesauro D, Mangiapia G, Pedone C, Morelli G. Nanostructures by self-assembling peptide amphiphile as potential selective drug carriers. Biopol Pep Sci. 2007;88(2):115–21.
17. Plow EF, Haas TA, Zhang L, Loftus J, Smith JW. Ligand binding to integrins. J Biol Chem. 2000;275(29):21785–8.
18. Desgrosellier JS, Barnes LA, Shields DJ, Huang M, Lau SK, Prévost N, *et al.* An integrin alpha(v)beta(3)-c-Src oncogenic unit promotes anchorage-independence and tumor progression. Nat Med. 2009;15(10):1163–9.
19. Cox D, Brennan M, Moran N. Integrins as therapeutic targets: lessons and opportunities. Nat Rev Drug Discov. 2010;9(10):804–20.
20. Hölig P, Bach M, Völkel T, Nahde T, Hoffmann S, Müller R, *et al.* Novel RGD lipopeptides for the targeting of liposomes to integrin-expressing endothelial and melanoma cells. Protein Eng Des Sel. 2004;17(5):433–41.
21. Shen SI, Kotamraj PR, Bhattacharya S, Li X, Jasti BR. Synthesis and characterization of RGD-fatty acid amphiphilic micelles as targeted delivery carriers for anticancer agents. J Drug Target. 2007;15(1):51–8.
22. Antunes P, Ginj M, Walter MA, Chen J, Reubi JC, Maecke HR. Influence of different spacers on the biological profile of a DOTA-somatostatin analogue. Bioconjug Chem. 2007;18(1):84–92.
23. Wasserheit C, Frazein A, Oratz R, Sorich J, Downey A, Hochster H, *et al.* Phase II trial of paclitaxel and cisplatin in women with advanced breast cancer: an active regimen with limiting neurotoxicity. J Clin Oncol. 1996;14(7):1993–9.
24. Weiss RB, Donehower RC, Wiernik PH, Ohnuma T, Gralla RJ, Trump DL, *et al.* Hypersensitivity reactions from taxol. J Clin Oncol. 1990;8(7):1263–8.
25. Zhan C, Gu B, Xie C, Li J, Liu Y, Lu W. Cyclic RGD conjugated poly(ethylene glycol)-co-poly(lactic acid) micelle enhances paclitaxel anti-glioblastoma effect. J Control Release. 2010;143(1):136–42.
26. Hu Z, Luo F, Pan Y, Hou C, Ren L, Chen J, *et al.* Arg-Gly-Asp (RGD) peptide conjugated poly(lactic acid)-poly(ethylene oxide) micelle for targeted drug delivery. J Biomed Mater Res A. 2008;85(3):797–807.
27. Jiang X, Sha X, Xin H, Chen L, Gao X, Wang X, *et al.* Self-aggregated pegylated poly (trimethylene carbonate) nanoparticles decorated with c(RGDyK) peptide for targeted paclitaxel delivery to integrin-rich tumors. Biomaterials. 2011;32(35):9457–69.
28. Danhier F, Vroman B, Lecouturier N, Crokart N, Pourcelle V, Freichels H, *et al.* Targeting of tumor endothelium by RGD-grafted PLGA-nanoparticles loaded with paclitaxel. J Control Release. 2009;140(2):166–73.
29. Sovadinova I, Palermo EF, Huang R, Thoma LM, Kuroda K. Mechanism of polymer-induced hemolysis: nanosized pore formation and osmotic lysis. Biomacromolecules. 2011;12(1):260–8.
30. Kotamraj P, Russu WA, Jasti B, Wu J, Li X. Novel integrin-targeted binding-triggered drug delivery system for methotrexate. Pharm Res. 2011;28(12):3208–19.
31. Tang R, Ji W, Wang C. Amphiphilic block copolymers bearing ortho ester side-chains: pH-dependent hydrolysis and self-assembly in water. Macromol Biosci. 2010;10(2):192–201.
32. Lee ES, Oh YT, Youn YS, Nam M, Park B, Yun J, *et al.* Binary mixing of micelles using Pluronics for a nano-sized drug delivery system. Colloids Surf B Biointerfaces. 2011;82(1):190–5.
33. Domínguez A, Fernández A, González N, Iglesias E, Montenegro L. Determination of critical micelle concentration of some surfactants by three techniques. J Chem Edu. 1997;74(10):1227–31.
34. Danhier F, Feron O, Préat V. To exploit the tumor microenvironment: passive and active tumor targeting of nanocarriers for anticancer drug delivery. J Control Release. 2010;148(2):135–46.
35. Ding H, Yong KT, Roy I, Hu R, Wu F, Zhao L, *et al.* Bioconjugated PLGA-4-arm-PEG branched polymeric nanoparticles as novel tumor targeting carriers. Nanotechology. 2011;22(16):165101.
36. Qui LY, Bae YH. Polymer architecture and drug delivery. Pharm Res. 2006;23(1):1–30.
37. Wang Y, Wang X, Zhang Y, Yang S, Wang J, Zhang X, *et al.* RGD-modified polymeric micelles as potential carriers for targeted delivery to integrin-overexpressing tumor vasculature and tumor cells. J Drug Target. 2009;179(6):459–67.
38. Chu-Kung AF, Nguyen R, Bozzelli KN, Tirrell M. Chain length dependence of antimicrobial peptide-fatty acid conjugate activity. J Colloid Interface Sci. 2010;345(2):160–7.
39. Koppelhus U, Shiraishi T, Zachar V, Pankratova S, Nielsen PE. Improved cellular activity of antisense peptide nucleic acids by conjugation to a cationic peptide-lipid (CatLip) domain. Bioconjug Chem. 2008;19(8):1526–34.
40. Bellmann-Sickert K, Elling CE, Madsen AN, Little PB, Lundgren K, Gerlach LO, *et al.* Long-acting lipidated analogue of human pancreatic polypeptide is slowly released into circulation. J Med Chem. 2011;54(8):2658–67.
41. Matsonand JB, Stupp SI. Drug release from hydrazone-containing peptide amphiphiles. Chem Commun (Camb). 2011;47(28):7962–4.
42. Kim JK, Anderson J, Jun HW, Repka MA, Jo S. Self-assembling peptide amphiphile-based nanofiber gel for bioresponsive cisplatin delivery. Mol Pharm. 2009;6(3):978–85.
43. Xiong JP, Stehle T, Zhang R, Joachimiak A, Frech M, Goodman SL, *et al.* Crystal structure of the extracellular segment of integrin alpha Vbeta3 in complex with an Arg-Gly-Asp ligand. Science. 2002;296(5565):151–5.
44. Zhang H, Schneider SE, Bray BL, Friedrich PE, Tvermoes NA, Mader CJ, *et al.* Process development of TRI-999, a fatty-acid modified hiv fusion inhibitory peptide. Org Process Res Dev. 2008;12(1):101–10.
45. Adams ML, Lavasanifar A, Kwon GS. Amphiphilic block copolymers for drug delivery. J Pharm Sci. 2003;92(7):1343–55.
46. Lee ES, Na K, Bae YH. Polymeric micelle for tumor pH and folate-mediated targeting. J Control Release. 2003;91(1–2):103–13.
47. Zhang Y, Wang X, Wang J, Zhang X, Zhang Q. Octreotide-modified polymeric micelles as potential carriers for targeted docetaxel delivery to somatostatin receptor overexpressing tumor cells. Pharm Res. 2011;28(5):1167–78.
48. Kedar U, Phutane P, Shidhaye S, Kadam V. Advances in polymeric micelles for drug delivery and tumor targeting. Nanomedicine. 2010;6(6):714–29.
49. Li S, Huang L. Pharmacokinetics and biodistribution of nanoparticles. Mol Pharm. 2008;5(4):496–504.
50. Alexis F, Pridgen E, Molnar LK, Farokhzad OC. Factors affecting the clearance and biodistribution of polymeric nanoparticles. Mol Pharm. 2008;5(4):505–15.
51. Castel S, Pagan R, Mitjans F, Piulats J, Goodman S, Jonczyek A, *et al.* RGD Peptides and monoclonal antibodies, antagonists of αv_Integrin, enter the cells by independent endocytic pathways. Lab Invest. 2001;81(12):1615–26.
52. Torchilin VP. Structure and design of polymeric surfactant-based drug delivery systems. J Control Release. 2001;73(2–3):137–72.
53. Chen H, Kim S, Li L, Wang S, Park K, Cheng JX. Release of hydrophobic molecules from polymer micelles into cell membranes revealed by förster resonance energy transfer imaging. PNAS. 2008;105(18):6596–601.
54. Chen H, Kim S, He W, Wang H, Low PS, Park K, *et al.* Fast release of lipophilic agents from circulating PEG-PDLLA micelles revealed by *in vivo* förster resonance energy transfer imaging. Langmuir. 2008;24(10):5213–7.
55. Lu J, Owen SC, Shoichet MS. Stability of self-assembled polymeric micelles in serum. Macromolecules. 2011;44(15):6002–8.
56. Yang C, Tan JPK, Cheng W, Attia ABE, Ting CTY, Nelson A, *et al.* Supramolecular nanostructures designed for high cargo loading capacity and kinetic stability. Nano Today. 2010;5(6):515–23.